ACS OMEGA

Article

http://pubs.acs.org/journal/acsodf

Seed-Induced Heterogeneous Cross-Seeding Self-Assembly of Human and Rat Islet Polypeptides

Rundong Hu,[†,⊥] Baiping Ren,[†,⊥] Mingzhen Zhang,[†] Hong Chen,[†] Yonglan Liu,[†] Lingyun Liu,[†] Xiong Gong,[‡] Binbo Jiang,[†,§] Jie Ma,[†,∥] and Jie Zheng*[,†]

[†]Department of Chemical and Biomolecular Engineering and [‡]College of Polymer Science and Polymer Engineering, The University of Akron, Akron, Ohio 44325, United States

[§]College of Chemical and Biological Engineering, Zhejiang University, Hangzhou, Zhejiang 310027, China

[∥]State Key Laboratory of Pollution Control and Resource Reuse, School of Environmental Science and Engineering, Tongji University, Shanghai 200092, China

ABSTRACT: Amyloid peptides can misfold and aggregate into amyloid oligomers and fibrils containing conformationally similar β-sheet structures, which are linked to the pathological hallmark of many neurodegenerative diseases. These β-sheet-rich amyloid aggregates provide common structural motifs to accelerate amyloid formation by acting as seeds. However, little is known about how one amyloid peptide aggregation will affect another one (namely, cross-seeding). In this work, we studied the cross-seeding possibility and efficiency between rat islet amyloid polypeptide (rIAPP) and human islet amyloid polypeptide (hIAPP) solution with preformed aggregates at different aggregation phases, using a combination of different biophysical techniques. hIAPP is a well-known peptide hormone that forms amyloid fibrils and induces cytotoxicity to β-cells in type 2 diabetes, whereas rIAPP is a nonaggregating and nontoxic peptide. Experimental results showed that all different preformed hIAPP aggregates can cross-seed rIAPP to promote the final fibril formation but exhibit different cross-seeding efficiencies. Evidently, hIAPP seeds preformed at a growth phase show the strongest cross-seeding potential to rIAPP, which accelerates the conformational transition from random structures to β-sheet and the aggregation process at the fibrillization stage. Homoseeding of hIAPP is more efficient in initiating and promoting aggregation than cross-seeding of hIAPP and rIAPP. Moreover, the cross-seeding of rIAPP with hIAPP at the lag phase also reduced cell viability, probably because of the formation of more toxic hybrid oligomers at the prolonged lag phase. The cross-seeding effects in this work may add new insights into the mechanistic understanding of the aggregation and coaggregation of amyloid peptides linked to different neurodegenerative diseases.

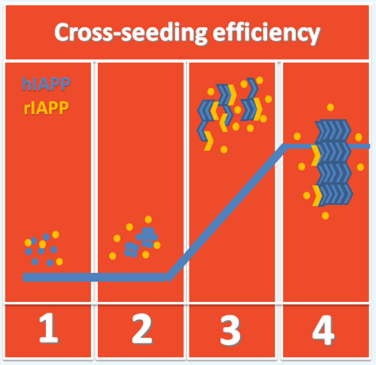

INTRODUCTION

Misfolding and aggregation of human islet amyloid polypeptide (hIAPP, also known as amylin) into amyloid fibrils, followed by subsequent deposition of these amyloid fibrils into pancreatic islets, are the neuropathological hallmark of type 2 diabetes (T2D).[1] hIAPP is a 37-residue peptide hormone synthesized by the pancreatic β-cells with physiological circulating concentrations ranging from 1.6 to 20 pM in nondiabetic people.[2] Amyloid formation by hIAPP is believed to be associated with β-cell death and dysfunction, the failure of islet transplantation, and the development of T2D. The hIAPP fibrillization process usually exhibits a typical three-stage sigmoidal kinetics,[3−5] starting with a lag phase where hIAPP monomers slowly accumulate into small seeds (commonly termed as small nucleus), followed by a growth phase where the small seeds act as catalysts to interact with monomers and rapidly grow into larger aggregates via peptide addition, and finally reaching an equilibrium phase where most of the aggregates convert into mature fibrils.[6−8] hIAPP aggregates not only increase their sizes and change their morphologies with time but also undergo the complex structural transition from random coil → α-helix → β-sheet with an increase in the β-sheet content.[9,10] Because the formation of nucleus seeds is a rate-determining step for hIAPP aggregation, the hIAPP fibrillization process is modeled using a seeding-dependent aggregation mechanism. This mechanism is also a general feature of amyloid formation by other amyloid peptides (e.g., Aβ, α-synuclein, and tau protein).[11] Moreover, small hIAPP seeds are often found to be highly toxic to cultured pancreatic islet β-cells and to islets.[12,13] Therefore, the study of seeding-induced amyloid aggregation and toxicity mechanisms is fundamentally and (pre)clinically important for therapeutic and prevention strategies against T2D.

In general, seeding a protein/peptide solution with preformed homogeneous aggregates can dramatically change (usually enhance) the growth rate of amyloids. Jarrett et al.[12,13] conducted comparative kinetic studies of Aβ aggregation to demonstrate their nucleation-dependent polymerization mechanisms. They found that the addition of Aβ preformed fibrils

Received: December 28, 2016
Accepted: February 20, 2017
Published: March 6, 2017

DOI: 10.1021/acsomega.6b00559
ACS Omega 2017, 2, 784−792

into initially soluble Aβ solutions eliminated the nucleation time and thus led to a rapid aggregation. Kayed et al.[14] utilized a variety of biochemical methods to study the nucleation−polymerization process for hIAPP amyloid formation in the presence of the preformed hIAPP seeds. Come et al.[15] studied the aggregation of a fragment of the prion protein (PrP) containing residues 96−111 in the absence and presence of PrP_{96-111} seeds. The seeded groups significantly reduced the lag-phase time and promoted fibril formation. All of these in vitro studies showed that the preformed homologous seeds indeed accelerate amyloid formation through bypassing the lag phase.[16]

In vivo studies further confirmed that amyloid proteins/peptides can spread the pathology between cells and tissues, and in some cases, they stimulate the disorder features when implemented into animal models through homogeneous seeding.[17] Luk et al.[18,19] found that an inoculation of synthetic α-synuclein fibrils into wild-type mice can elicit a massive formation and subsequent cell-to-cell transmission of pathological α-synuclein via the murine central nervous system. Consequently, such amyloid pathology accumulation generated a progressive loss of neurons and culminated in motor deficit in originally healthy mice. Kane et al.[20] performed the seeding experiment by injecting Alzheimer brain extracts intracerebrally into the Aβ precursor protein (APP) transgenic mice. A sharp contrast between the profuse presence of Aβ plaques in a tissue-injected mice group and the nonexistence of Aβ deposits in an uninjected mice group showed that Aβ can be seeded in vivo. Holmes et al.[21] developed a Fluorescence resonance energy transfer (FRET)-based biosensor to study the onset and progression of tau pathology using tau seeds in transgenic mice. They found that tau seeds can transmit from cell to cell via neural connections. All of these in vivo data indicated that seeding likely acted as an infectious agent to self-propagate different amyloid diseases including Alzheimer's disease (AD),[20] Parkinson disease,[18] and tauopathies.[21]

In a broader view, the seeding process could be homologous or heterologous. Several studies[22−24] reported the binding and coaggregation of different amyloid peptides, a process known as cross-seeding. Because most of the amyloid peptides share similar aggregation kinetics and structures, it is possible that amyloid seeding induces both homologous and heterologous amyloid formation. For example, α-synuclein fibrils could induce tau aggregation[25,26] in AD[22,23] and huntingtin aggregation in Huntington disease.[27] Similarly, intravenous injection of preformed fibrils of hIAPP or Aβ into hIAPP transgenic mice can act as seeds to stimulate hIAPP amyloids in the islet of Langerhans, and this finding supports that both seeding and cross-seeding can occur at local islets via blood.[26] To clarify the molecular requirements for peptide compatibility and the mechanisms behind them, a range of amyloid peptides were paired to study their cross-seeding behaviors in vitro. Kapurniotu and co-workers[28,29] studied the aggregation kinetics of amyloid fibrils formed by pure $Aβ_{40}$, pure hIAPP, and mixtures of both peptides at a molar ratio of 1:1. They found that both nucleation and fibrillization of Aβ−hIAPP mixtures were delayed as compared with the aggregation kinetics of pure Aβ or pure hIAPP. They concluded that the cross-seeding of Aβ−hIAPP and the homoseeding of Aβ and hIAPP likely occur in a competitive manner. Mandal et al.[30] performed multidimensional NMR to study the interaction between Aβ and α-synuclein in a membrane-mimic environment. Aβ and α-synuclein appeared to strongly interact with each other and mutually promote their respective amyloid fibrillization. Giasson et al.[31] also observed that the coincubation of α-synuclein and tau led to a synergistic fibrillization promotion of both peptides. Growing evidence from clinical studies[32,33] also showed the coexistence of different amyloid protein aggregates in one disease and of different amyloid diseases in the same individual, suggesting a direct interaction between different amyloid peptides.[34]

On the other hand, not any two different amyloid peptides can cross-seed each other. Aβ fibrils efficiently cross-seeded hIAPP in solution, whereas hIAPP fibrils did not cross-seed Aβ effectively, with only 2% of cross-seeding efficiency.[35] Similarly, transthyretin decreased Aβ deposition and suppressed cognitive deficits in AD mouse models.[36,37] It seems that the cross-seeding efficiency depends on the structural similarity between seeds and the other amyloid aggregates. It is likely that targeting peptides adopt a structure, at least partially identical to seeds, for amyloid growth. Although the results collected from literature point to the more complex mechanisms for amyloid cross-seeding, which remain to be answered, they also suggest that the cross-seeding is generally specific, and some cross-seeding barriers could exist because of the mismatch of sequences and structures between different amyloid peptides.

Completely different from hIAPP, rIAPP does not form amyloid peptides and is nontoxic to β-cells, although rIAPP differs from hIAPP only at six residues (H18R, F23L, A25P, I26V, S28P, and S29P)[38] (Scheme 1). Our previous molecular

Scheme 1. Sequence Comparison between Full-Length hIAPP and rIAPP, Where Dashed Boxes Highlight Six Different Amino Acids between hIAPP and rIAPP[a]

[a]Color ID: charged residues in purple, polar residues in green, and hydrophobic residues in brown.

dynamics simulation[39,40] showed that hIAPP and rIAPP can interact with each other to form hybrid structures via peptide elongation and lateral association. An exploration into this contrast amyloidogenic property between two nearly same sequences could be a big step toward a better understanding of amyloidosis and finding potential amyloid-prevention methods. In our previous work,[41] we studied the cross-sequence interaction between full-length $hIAPP_{37}$ and $rIAPP_{37}$. Our previous data showed that when coincubating $rIAPP_{37}$ with $hIAPP_{37}$, both in freshly prepared monomer states, rIAPP initially inhibited hIAPP aggregation at both lag and growth phases, but once the aggregation-promoting hIAPP nuclei or oligomers were formed, they could recruit and cross-seed rIAPP to promote final fibril formation. However, little is known about how different hIAPP seeds interact with rIAPP and about the toxicity of hIAPP/rIAPP complexes. Different from our previous work, here, we studied the homoseeding of hIAPP and the cross-seeding of rIAPP with preformed hIAPP seeds at different aggregation stages using combined experimental methods. The results showed that hIAPP seeds formed at different stages can not only seed hIAPP but can also cross-seed rIAPP, but the homologous seeding of hIAPP itself was more effective than the heterologous seeding of hIAPP with rIAPP. The different seeding and cross-seeding efficiencies also

DOI: 10.1021/acsomega.6b00559
ACS Omega 2017, 2, 784−792

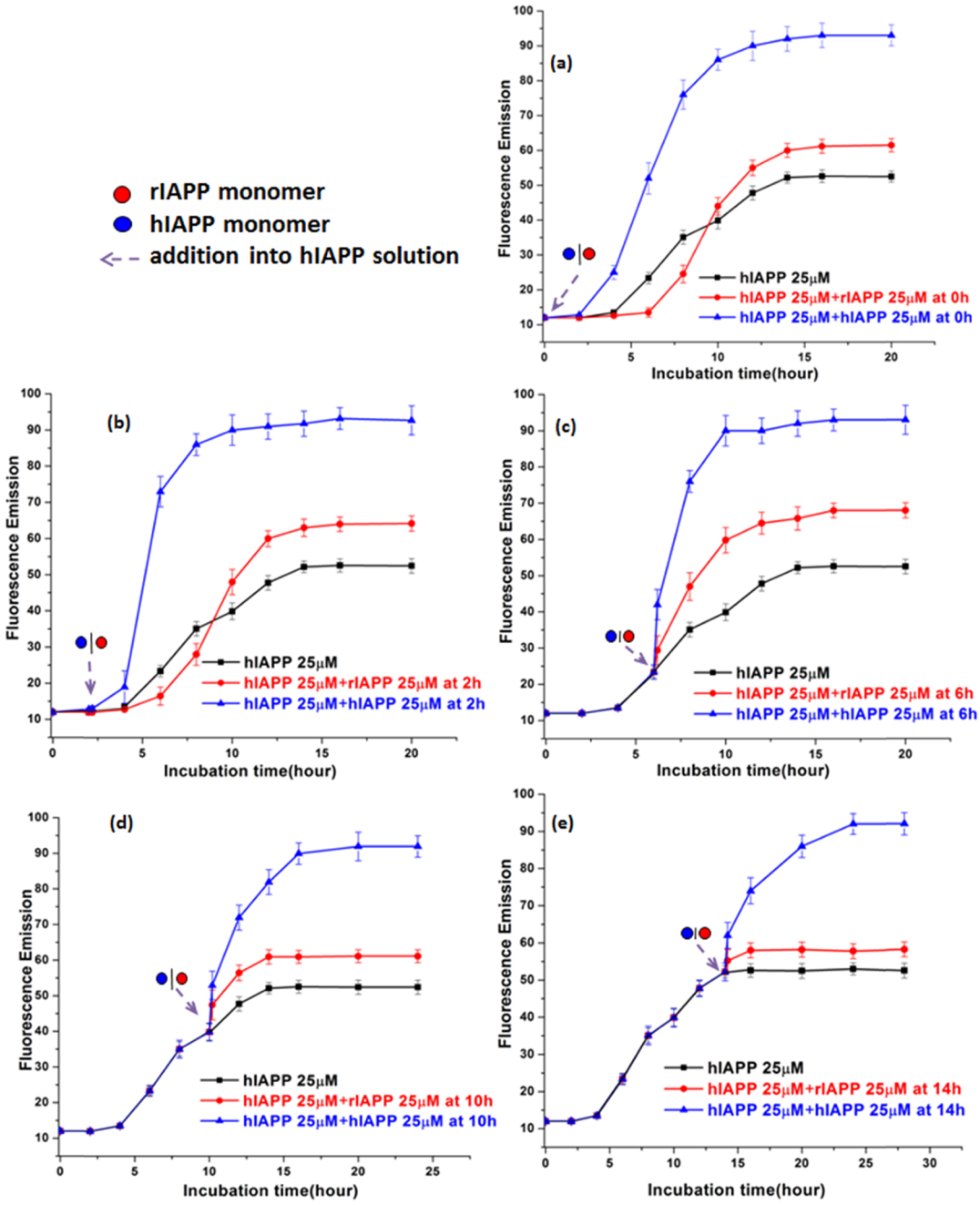

Figure 1. ThT aggregation kinetics for pure hIAPP (25 μM), cross-seeding by adding freshly prepared rIAPP (25 μM) to different hIAPP seeds preform at different time points, and homoseeding by adding freshly prepared hIAPP (25 μM) to different hIAPP seeds preform at different time points of (a) 0 h, (b) 2 h, (c) 6 h, (d) 10 h, and (e) 14 h, respectively. Arrows indicate the time point to add freshly prepared hIAPP or rIAPP. Error bars represent the average of three replicate experiments.

reflect a fact that there exists a cross-seeding barrier probably due to the mismatch of cross-seeding structures.

RESULTS AND DISCUSSION

Cross-Seeding of rIAPP and Homoseeding of hIAPP by Different hIAPP Seeds. Thioflavin T (ThT) fluorescence aggregation assays were used to assess the seeding of hIAPP and the cross-seeding of rIAPP in the presence of different preformed hIAPP aggregates. The assays were performed by adding freshly prepared hIAPP (25 μM) or rIAPP (25 μM) to the ongoing incubation (preaggregated) hIAPP solution (25 μM) at different time points (0, 2, 6, 10, and 14 h). This design is equivalent to using different hIAPP seeds formed at three different aggregation stages to seed the same species of hIAPP or cross-seed different species of rIAPP. ThT fluorescence intensities (excitation at 450 nm and emission at 490 ± 10 nm) were recorded every 2 h to monitor aggregate formation. As a control, pure hIAPP aggregation exhibited a typical sigmoidal nucleation−polymerization curve, starting with a lag phase of 0−4 h, followed by a rapid growth phase from 4−20 h, and ending at a stable plateau with a maximum ThT intensity of ∼52 after 20 h. Pure rIAPP under the same incubation conditions did not aggregate in solution, as evidenced by the absence of any ThT signal.[41]

DOI: 10.1021/acsomega.6b00559
ACS Omega 2017, 2, 784−792

First, we studied the cross-seeding behavior of rIAPP in the presence of different hIAPP seeds obtained from the nucleation, growth, and final equilibrium phases. Figure 1a (red line) shows that when coincubating both freshly prepared hIAPP (25 μM) and rIAPP (25 μM) together at 0 h, the lag time was prolonged to ∼6 h, whereas the growth rate was almost unchanged between 6 and 10 h and then increased after 10 h. Finally, the maximal ThT intensity reached a stable plateau of ∼61, which is ∼22.2% higher than that of pure hIAPP without adding rIAPP. Similarly, adding rIAPP to a seeded hIAPP solution at 2 h also increased the lag time to 5 h and promoted fibril formation with the maximum ThT intensity of ∼64 (Figure 1b). This result indicates that the introduction of rIAPP to the hIAPP solution at the nucleation stage slows down the seed formation and early aggregation of hIAPP, but once hIAPP seeds are formed, they can cross-seed rIAPP to form more fibrils. Then, we examined the cross-seeding of rIAPP using the hIAPP seed solution at the growth phase. In Figure 1c, 15 min after the addition of rIAPP to the 6-h-seeded hIAPP solutions, the aggregation rate was accelerated, as indicated by immediate ThT signal enhancement followed by a deeper slope at the growth phase. A similar burst of cross-seeding was also observed when adding rIAPP to a 10-h-seeded hIAPP solution, but the growth rate seemed not to change much (Figure 1d). Finally, when adding rIAPP to the preformed hIAPP fibrils at a final plateau stage of 14 h, the cross-seeding between rIAPP and hIAPP still occurred, but the acceleration of aggregation was much less than those found for preformed hIAPP aggregates at the nucleation and growth phases (Figure 1e), indicating that hIAPP aggregated states before the formation of large hIAPP fibrils are the major causative agent of cross-seeding. Moreover, in all cross-seeding tests containing the same amount of hIAPP and rIAPP (25 μM), because rIAPP alone does not aggregate and form amyloid fibrils, during the cross-seeding process, any increase in the final ThT intensity does not result from hIAPP fibrils alone but instead results from new hybrid hIAPP/rIAPP fibrils.

To further quantitatively compare the cross-seeding efficiency induced by different hIAPP seeds that were preformed at different aggregation stages, we summarized the increase in final ThT intensities for all cross-seeding tests relative to the final ThT intensity of pure hIAPP alone. As shown in Table 1, different preformed hIAPP aggregates can all cross-seed rIAPP to promote final fibril formation but they also exhibited different cross-seeding efficiencies. hIAPP aggregates, which were preformed at a growth phase of ∼6 h, showed the strongest cross-seeding potential to rIAPP. Evidently, the coaggregation and the cofibrillization of hIAPP and rIAPP were accelerated, leading to a 36.2% increase in amyloid fibrils, as reflected by the final ThT intensity enhancement. The cross-seeding between freshly prepared rIAPP and hIAPP aggregates preformed at the nucleation phase still led to 22−29% increase in the total amount of amyloid fibrils. Early hIAPP aggregates may contain more disordered structures, so the cross-seeding activities were reduced because of a greater extent of structural mismatch between hIAPP seeds and rIAPP. This is also confirmed by the delay of lag phase due to cross-seeding, where the introduction of rIAPP clearly interferes with the nuclei formation of hIAPP. Using hIAPP (proto)fibrils as the seeds where β-sheet structures dominate, the cross-seeding activity was not as effective as the optimal one. It is possible that hIAPP protofibrils or fibrils offer fewer active surface sites, particularly hydrophobic aggregation sites, to interact with rIAPP because these active sites have already been preoccupied by hIAPP.

Table 1. Summary of the Aggregation Kinetics for the Cross-Seeding of hIAPP and rIAPP[a]

	lag phase time change caused by monomer addition[c]		final fibril change caused by monomer addition[d]	
addition of rIAPP or hIAPP monomers to the hIAPP solution[b]	rIAPP monomer addition	hIAPP monomer addition	rIAPP monomer addition (%)	hIAPP monomer addition (%)
addition at 0 h	+2 h	−2 h	22.20	99.50
addition at 2 h	+1 h	−1.5 h	28.90	98.90
addition at 6 h	N/A	N/A	36.20	100.10
addition at 10 h	N/A	N/A	21.50	99.80
addition at 14 h	N/A	N/A	14.10	99.50

[a]Data were extracted from the ThT curves in Figure 1. [b]Freshly prepared rIAPP or hIAPP monomers (25 μM) were added to the pure hIAPP solution (25 μM) seeded at different time points of 0−14 h. [c]Using the 0−4 h of pure hIAPP aggregation as a lag phase, the addition of rIAPP (hIAPP) monomer to the seeded hIAPP solution induces the increase (decrease) of the lag phase. [d]Using the final ThT plateau of pure hIAPP aggregation as an indicator of fibrils being formed, the addition of rIAPP (hIAPP) monomer to all seeded hIAPP solution induces the increase in final fibril formation.

In parallel, we also examined the seeding behavior of hIAPP for comparison using the same cross-seeding protocols and conditions. We added freshly prepared hIAPP monomers to hIAPP solutions seeded at different times and then monitored the aggregation kinetics changes before and after adding hIAPP monomers by recording ThT signals. In Figure 1a, the addition of 25 μM hIAPP to another 25 μM hIAPP solution at 0 h is equivalent to the incubation of freshly prepared 50 μM hIAPP monomers at 0 h, whose aggregation curve should be different from that of 25 μM hIAPP itself, as shown in Figure 1a. As compared to a control group of 25 μM hIAPP, the double concentration group of 25 hIAPP + 25 hIAPP (50 μM) exhibited faster nucleation at the lag phase and more fibrils being formed at the final phase. Moreover, homoseeding in the 25 hIAPP + 25 hIAPP group is more efficient than cross-seeding in the 25 hIAPP + 25 rIAPP group. In both cases of the homoseeding initiated at the nucleation phase, the hIAPP aggregation showed faster kinetics with a short lag phase of 2 h. This is different from cross-seeding that leads to a prolonged lag phase. In the other cases of mixing hIAPP monomers with preformed hIAPP seeds at the growth and equilibrium phases, there were immediate burst aggregations, followed by a faster aggregation to achieve higher ThT plateaus. These home-seeding data showed trends similar to the cross-seeding data, but the final ThT intensities of homoseeding mixtures were always higher than those of cross-seeding mixtures at the same peptide concentrations. It is also possible that both coaggregation and homoseeding can occur at the same time, leading to a faster aggregation process. Moreover, we also found that there were no statistical differences in the final ThT intensity for all homoseeding groups, which is another distinctive feature between hIAPP homoseeding and hIAPP/rIAPP cross-seeding. The homoseeding efficiency of hIAPP itself appears not to be necessarily relied on the preaggregated state of homoseeds, although its seeding-induced aggregation rate still does. By contrast, the cross-seeding process involves a critical step for rIAPP being converted into an amyloidlike structure, and this transformation is believed to largely depend

DOI: 10.1021/acsomega.6b00559
ACS Omega 2017, 2, 784−792

on the hIAPP-seed condition. From the sequence perspective, the high amyloidogenic property of the hIAPP (20−29) region has been demonstrated. Peptide fragments from this hIAPP (20-29), for example, $_{22}$NFGAILSS$_{29}$,[42] $_{22}$NFGAIL$_{27}$,[43] and $_{24}$GAILSS$_{29}$[44] can independently assemble into amyloid fibrils similar to full-length hIAPP fibrils. Differently, for the rIAPP peptide, the presence of three proline residues located in the 24−29 region (GPVLPP) is believed to disrupt the amyloidogenic property and reduce the β-sheet formation.[45,46] The presence of hIAPP seeds may alter the folding pathway of rIAPP and drive rIAPP to be incorporated into hIAPP seeds. It is also possible that the N-terminal β-sheet of hIAPP aggregates could serve as a template interface either to recruit and accommodate rIAPP with a conformationally similar N-terminal β-sheet (not the C-terminal 20−29 region) or to facilitate the structural transition of rIAPP to partially fold into compatible β-sheet structures.

A comparison of homoseeding and cross-seeding ThT data reveals some similarities and differences. First, hIAPP at different aggregation phases can always seed hIAPP monomers and cross-seed rIAPP monomers, but the homoseeding/cross-seeding efficacies seem to be more dependent on the aggregation-prone intermediate species. The population of hIAPP intermediate species, not those species at the initial nucleation and final equilibrate phases, is more critical to achieve high coaggregation and homo-/cross-seeding. These hIAPP intermediate species are largely partially folded with some solvent-exposed hydrophobic moieties that promote intermolecular interactions with hIAPP or rIAPP. Second, homoseeding is more efficient in initiating and promoting aggregation than cross-seeding. This is not surprising because mismatch sequences between hIAPP and rIAPP increases energy barriers for efficient cross-interactions.

Cross-Seeding Induces Structural Changes in Amyloid Aggregates. To gain further insights into cross-seeding, we monitored the structural changes of cross-seeded hIAPP/rIAPP aggregates using atomic force microscopy (AFM) and circular dichroism (CD) under the exact same conditions used in ThT tests. Figure 2 shows the representative AFM images of the cross-seeding of fresh rIAPP monomers with hIAPP solutions seeded for different times. As a control, AFM images of pure hIAPP aggregation (25 μM) showed typical amyloid morphologies at different aggregation phases, confirming the conversion of small oligomers into higher-order amyloid fibrils. The widths of most hIAPP fibrils were similar and ranged between 8 and 12 nm. CD spectroscopy images in Figure 3 also showed that pure hIAPP experienced a typical structural transition from the initial random coil to the β-sheet structure, as indicated by the appearance of the two peaks at 195 and 215 nm, both of which corresponds to the β-sheet structure. For comparison, when coincubating equimolar hIAPP and rIAPP monomers at 0 h, it is clear that the lag phase was prolonged to 4 h, during which a large amount of spherical aggregates of 1−2 nm diameters were predominated. Therefore, the prolonged lag phase indicates the occurrence of coaggregation between hIAPP and rIAPP. After that, short, thin protofibrils and long, thicker mature fibrils were observed at 8 and 16 h, respectively. Their morphologies were almost identical to those of pure hIAPP (proto)fibrils. Moreover, upon cross-seeding rIAPP by preformed hIAPP seeds at different time points of 2−14 h, AFM images in all cases consistently showed the morphological changes from small aggregates, low density protofibrils, to highly dense fibrils, and the final morphologies

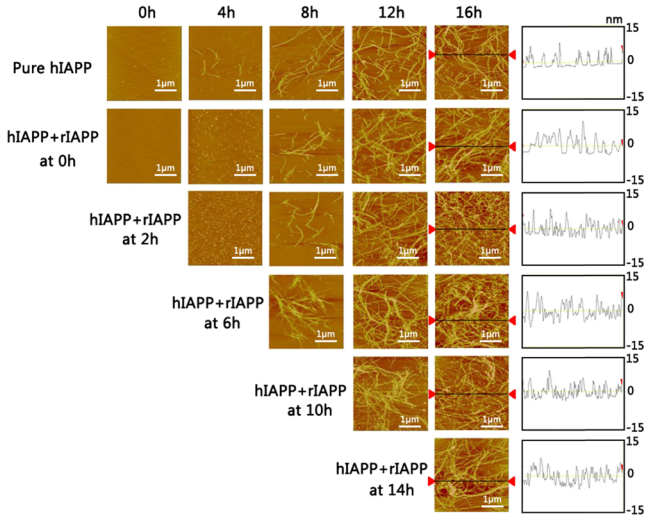

Figure 2. AFM images for pure hIAPP (25 μM, the first row) and cross-seeding of hIAPP (25 μM)/rIAPP (25 μM) captured at different time points of 0, 4, 8, 12, and 16 h. The notation of "hIAPP + rIAPP at 0, 2, 6, 10, and 14 h" indicates the different time points to add freshly prepared rIAPP monomers to the seeded hIAPP solution. The height analysis for the final amyloid fibrils for each group is also provided.

(a)

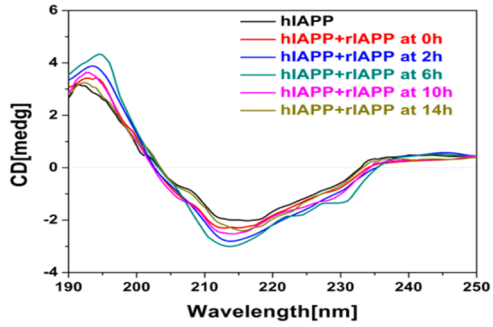

(b)

	α-helix %	β-sheet %	Other (disordered) %
hIAPP	46.0	30.2	23.8
hIAPP+rIAPP at 0h	35.9	44.8	19.3
hIAPP+rIAPP at 2h	32.0	47.8	20.2
hIAPP+rIAPP at 6h	30.8	51.1	18.1
hIAPP+rIAPP at 10h	36.8	44.0	19.2
hIAPP+rIAPP at 14h	37.4	37.3	25.3

Figure 3. (a) Final far-UV CD spectra for pure hIAPP (25 μM) and cross-seeding of hIAPP (25 μM)/rIAPP (25 μM) where freshly prepared rIAPP was added to the seeded hIAPP solution at 0, 2, 6, 10, and 14 h. The signals of cross-seeding groups were subtracted by a background signal produced by pure rIAPP. (b) Final secondary structure distribution of pure hIAPP (25 μM) and the cross-seeding of hIAPP (25 μM)/rIAPP (25 μM) using the CDSSTR method.

of cross-seeded fibrils were found to be similar to those of homoseeded fibrils. Height profiles obtained from the AFM images showed that all amyloid fibrils exhibited similar heights of 5−15 nm. The AFM results were also supported by our recent simulation work[39] that hIAPP/rIAPP assemblies reflected a polymorphic nature of cross-seeding species, that is, hIAPP can cross interact with rIAPP to form hybrid amyloid

DOI: 10.1021/acsomega.6b00559
ACS Omega 2017, 2, 784−792

aggregates and fibrils via two pathways of peptide elongation and lateral association.

Additionally, we conducted CD experiments for secondary structure characterization of the fibrils generated through cross-seeding. Considering that rIAPP has the same concentration of hIAPP and rIAPP itself mainly adopts random coil conformations, in the cross-seeding cases studied, we found that the adsorption spectra of cross-seeding samples were largely dominated by a strong negative peak at ∼197 nm, corresponding to major random coil conformations. This makes the other combined secondary structures difficult to characterize, particularly a characteristic peak of β-sheet at ∼195 nm. To address this issue, all raw CD curves of cross-seeding samples recorded at the end of the reaction (24 h) were corrected by subtracting a control curve of pure rIAPP. In this way, the corrected curves should present a linear superposition of hIAPP conformations and transformed rIAPP conformations. In Figure 3, the CD spectrum of the final hIAPP fibrils showed a positive peak at ∼192 nm and a negative valley at ∼210 nm, confirming the β-sheet-rich structure of pure hIAPP. Upon cross-seeding with rIAPP, all corrected CD curves not only shifted their positive peaks to ∼195 nm with enhanced magnitude but also deepened the negative peaks. The continuous shift and the increase in the peaks indicate that cross-seeding continues to develop β-sheet-rich fibrils. On the basis of the entire CD spectrum, we performed CDpro analysis to obtain the final secondary structure content of pure hIAPP and cross-seeded hIAPP/rIAPP samples using the CDSSTR (Circular dichroism standardized stepwise treatment regimen) method (Figure 3b). As compared with the pure hIAPP group containing ∼46% of α-helix and ∼30% of β-sheet after 20 h incubation, all cross-seedings of hIAPP/rIAPP groups incubated at different time points resulted in higher β-sheet of 37−51% and lower α-helix of ∼31−37%. This suggests that the cross-seeding of hIAPP/rIAPP induces an increase in β-sheet content at the expense of structural conversion of α-helical or random structures. Moreover, considering the two facts that (1) pure rIAPP peptides do not produce any ThT signal and (2) the same amount of hIAPP (25 μM) was used in all tested cross-seeding cases, any increase in the final ThT intensity actually does not result from hIAPP fibrils but instead results from new hybrid hIAPP/rIAPP fibrils (Figure 1). Second, because rIAPP always retains its random coil conformation, the difference in CD spectrum between the hIAPP/rIAPP mixtures and pure hIAPP is likely induced by the incorporated rIAPP (Figure 3). Taken together, collective data from ThT, AFM, and CD analyses confirm the occurrence of cross-seeding between hIAPP and rIAPP.

Cross-Seeding Increases Cell Toxicity. To examine whether the cross-seeding aggregates are innocuous, we conducted a cell viability experiment using the MTT assay with the RIN-m5f cell line (Figure 4). To establish a baseline, the absorbance of the RIN-m5f cell media alone was measured, and the value was set as 100% of cells being viable. When incubating pure hIAPP (25 μM) with cell culture media for 48 h, the cell viability decreased to 65% of that of the control, confirming that hIAPP aggregates are toxic to cells. By contrast, pure rIAPP (25 μM) presented very low cytotoxicity to cells, as evidenced by the 97.5% cell viability during 48 h of cell culture. In all cross-seeding tests, the cell viability was reduced as compared with that of the control, but the extent of cell viability showed an increasing trend as a function of time point

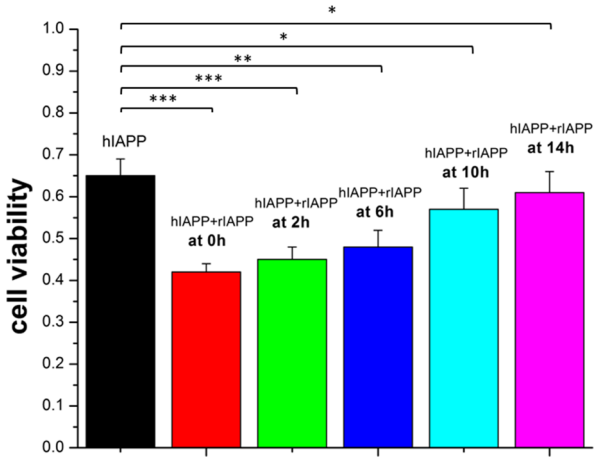

Figure 4. RIN-m5F cell viability, as determined by the MTT assay, in the presence of pure hIAPP (25 μM) and the cross-seeding of hIAPP (25 μM)/rIAPP (25 μM), where freshly prepared rIAPP was added to the seeded hIAPP solution at 0, 2, 6, 10, and 14 h. The cross-seeding of hIAPP/rIAPP decreases cell viability. ***: $p < 0.001$; **: $p < 0.01$; *: $p < 0.05$, vs pure hIAPP.

for adding rIAPP to the seeded hIAPP solution. Specifically, when introducing rIAPP to the hIAPP solution at early aggregation time points of 0, 2, and 6 h, the cross-seeding aggregates ultimately led to a high toxicity ranging from 58 to 52%. As confirmed by ThT and AFM, the cross-seeding of rIAPP with hIAPP at the lag phase (0−2 h) extends the nucleation stage and thus produces the more predominant oligomers that are highly toxic and also prolongs their lifetime. In comparison, when using the hIAPP fibrillar aggregates preformed at the later aggregation stages (14 h) to cross-seed rIAPP, the cell viability was ∼60%, which was slightly lower than the 65% cell viability induced by pure hIAPP. It is generally accepted that small, soluble amyloid oligomers are the most toxic species as compared with insoluble final amyloid fibrils.[47] When adding rIAPP monomers to the preformed hIAPP protofibrils, hIAPP/rIAPP oligomers are unlikely to form because of the absence of hIAPP oligomers. Instead, hIAPP protofibrils will recruit rIAPP monomers to form large hIAPP/rIAPP protofibrils. Such a cross-seeding effect would reduce the formation of the potential toxic hIAPP/rIAPP oligomers but promote the formation of less toxic hybrid hIAPP/rIAPP fibrils, both of which lead to the increase in cell viability.

CONCLUSIONS

hIAPP and rIAPP have completely opposite aggregation propensities, with only six residue differences in their sequences. hIAPP is known as the causal agent to induce T2D via its strong aggregation and toxic properties, whereas rIAPP is not. The cross-seeding of these two different peptides is fundamentally important for understanding the mechanism of hIAPP aggregation linked to T2D but remains elusive. To address this unexplored fundamental issue, here, we have studied the effect of cross-seeding between rIAPP monomers and different hIAPP seeds on aggregation kinetics, structure, and toxicity in vitro. In all cases of cross-seeding, the hIAPP solution containing different preformed seeds can indeed cross-seed rIAPP to promote final amyloid fibril formation. But, the cross-seeding activity was strongly depended on hIAPP seeds. Specifically, hIAPP seeds formed at the growth phase exhibited

DOI: 10.1021/acsomega.6b00559
ACS Omega 2017, 2, 784−792

the best cross-seeding capacity for rIAPP where the coaggregation and cofibrillization of hIAPP and rIAPP were accelerated, whereas hIAPP fibrillar seeds exhibited poor cross-seeding capacity. For the toxicity tests, all cross-seedings of rIAPP with different hIAPP seeds induced a higher cell toxicity than pure hIAPP. Particularly, in the case of using hIAPP seeds formed at the nucleation stage to cross-seed rIAPP, the lag phase was retarded, which elevated the production of more toxic intermediates and thus caused the highest cell toxicity. Moreover, the comparison of homo- and cross-seeding aggregation kinetics showed that the homoseeding of hIAPP is more efficient to promote amyloid aggregation than the cross-seeding of hIAPP and rIAPP. This study demonstrates the cross-seeding between strong-aggregation hIAPP and nonaggregation rIAPP, which may provide some clues to better understand the mechanisms of amyloidogenesis.

METHODS AND MATERIALS

Reagents. 1,1,1,3,3,3-Hexafluoro-2-propanol (HFIP, ≥99.9%), dimethyl sulfoxide (DMSO, ≥99.9%), 10 mM phosphate-buffered saline (PBS) (pH = 7.4), 10 mM NaOH, and ThT (98%) were purchased from Sigma-Aldrich (St. Louis, MO). hIAPP (1-37) (≥95.0%) and rIAPP (1-37) (≥95.0%) were purchased from American Peptide Inc. (Sunnyvale, CA). All other chemicals were of the highest grade available.

Peptide Purification and Preparation. Both IAPP peptides were obtained in a lyophilized form and stored at −20 °C as arrived. To prepare the monomeric peptide solution, 1.0 mg of each preaggregated peptide was dissolved in HFIP for 2 h, sonicated for 30 min to remove any preexisting aggregates or seeds, and centrifuged at 14 000 rpm for 30 min at 4 °C. The top peptide (80%) solution was then extracted, subpackaged, frozen with liquid nitrogen, and then dried using a freeze-dryer. The dry peptide powder was lyophilized at −80 °C and used within 1 week. Purified hIAPP powder (0.2 mg) was aliquoted in 30 μL of 10 mM NaOH solution and sonicated for 1 min to obtain a homogenous solution. The initiation of hIAPP (25 μM) aggregation in solution was accomplished by adding 30 μL of the obtained NaOH−hIAPP solution to 2 mL of 10 mM PBS buffer. Then, for the hIAPP/rIAPP solution mixed in different stages, we used the same protocol to prepare initial pure hIAPP solutions at the beginning and added 30 μL of fresh NaOH−rIAPP solutions to each pure hIAPP solution at 0, 2, 6, 10, and 14 h. All solutions were incubated at 37 °C.

ThT Fluorescence Assay. ThT fluorescence assay is considered to be a standard method to detect the formation of amyloid fibrils because ThT can specifically bind to the β-sheet structure of protein fibrils and gives a strong fluorescence emission. A ThT solution (2 mM) was prepared by adding 0.033 g of ThT powder into 50 mL of deionized (DI) water. The resultant 250 μL of the 2 mM ThT solution was further diluted in 50 mL of Tris buffer (pH = 7.4) to a final concentration of 10 μM. The peptide solution (60 μL) was added into the 10 μM ThT−Tris solution (3 mL) at each time point. Fluorescence spectra were recorded using an LS-55 fluorescence spectrometer (Perkin-Elmer Corp., Waltham, MA). All measurements were carried out in aqueous solution using a 1 × 1 cm^2 quartz cuvette. The ThT fluorescence emission wavelengths were recorded between 470 and 500 nm with an excitation wavelength of 450 nm. Each experiment was repeated at least three times, and each sample was tested in quintuplicates.

CD Spectroscopy. The secondary structures of hIAPP and rIAPP in solution were examined by CD spectroscopy using a J-1500 spectropolarimeter (Jasco Inc., Japan) in the continuous scanning mode at room temperature. Peptide solutions incubated for 20 h (160 μL for each time point) were placed into a rectangular quartz cuvette of a 1 mm pathlength without dilution. The spectra were recorded between 250 and 190 nm at a 0.5 nm resolution and a 50 nm/min scan rate. All spectra were corrected by subtracting the baseline and averaged by three successive scans for each sample.

Tapping-Mode AFM. The morphology changes of peptides during fibrillization were monitored by tapping-mode AFM. The sample (20 μL) used in both ThT fluorescence assay and CD spectrum test was taken for the AFM measurement at different time points to correlate the hIAPP or rIAPP morphology changes with their growth kinetics. A peptide solution was deposited onto a freshly cleaved mica substrate for 1 min, rinsed three times with 50 mL of DI water to remove the salts and loosely bound peptide, and dried with compressed air for 5 min before AFM imaging. Tapping-mode AFM imaging was performed in air using a Nanoscope III multimode scanning probe microscope (Veeco Corp., Santa Barbara, CA) equipped with a 15 μm E scanner. Commercial Si cantilevers (Nanoscience) with an elastic modulus of 40 N m^{-1} were used. All images were acquired as 512 × 512 pixel images at a typical scan rate of 1.0−2.0 Hz with a vertical-tip oscillation frequency of ∼160 kHz. Representative AFM images were obtained by scanning at least six different locations of different samples.

Cell Culture. Rat insulinoma (RIN-m5F) cells (ATCC, Manassas, VA) were used as model pancreatic β-cells and cultured in 75 cm^2 T-flasks in sterile-filtered RPMI-1640 medium (ATCC, Manassas, VA) containing 10% fetal bovine serum (ATCC, Manassas, VA) and 1% penicillin/streptomycin (ATCC, Manassas, VA). The flasks were incubated in a humidified incubator with 5% CO_2 at 37 °C. Cells were then cultured to confluence and harvested using a 0.25% Trypsin−EDTA (1×) solution (Lonza, Walkersville, MD). The cells were counted using a hemocytometer and plated in a 96-well tissue culture plate at 50 000 cells per well in 100 μL of medium, which allow them to attach inside of the incubator for 24 h.

MTT Toxicity Assay. MTT-based cell toxicity assays were performed to assess the cytotoxicity of hIAPP and rIAPP assemblies. A 96-well plate with cells was split into seven groups, with each group containing 12 replicates. The first group containing cells only in the medium was used as a positive control. NaOH−hIAPP solutions diluted by the cell medium were added to groups 2−7 to achieve the 25 μM final concentrations. The cells were then incubated for another 48 h. During the first 24 h, we used the same protocol to prepare NaOH−rIAPP solutions and added them to each pure hIAPP incubation solution (groups 3−7) at 0, 2, 6, 10, and 14 h. MTT (5 mg) was dissolved in sterile PBS solution (1 mL). Then, we mixed this MTT−PBS solution with 10 mL of the cell medium. The original cell medium was removed, and 100 μL of this MTT−PBS-medium solution was added to each well. The cells were incubated for 4 h at 37 °C to convert MTT to formazan crystals. After that, the entire 100 μL of the MTT−PBS-medium solution was removed from each well. Formazan crystals formed at the bottom of each well were dissolved by adding 100 μL of DMSO per well and were thoroughly mixed. The cells were incubated for an additional 10 min at 37 °C and mixed again to ensure that the formazan was fully dissolved.

DOI: 10.1021/acsomega.6b00559
ACS Omega 2017, 2, 784−792

The plates were placed in a Synergy H1 microplate reader (BioTek, Winooski, VT), and the absorbance was read at 540 nm to determine the formazan content. The sample absorbance was then compared with the control groups to determine cell viability. All statistical data were expressed as mean ± standard deviation. Statistical analysis of all data was performed using one-way analysis of variance and Tukey's test. p values <0.05 were considered to be statistically significant.

AUTHOR INFORMATION

Corresponding Author

*E-mail: zhengj@uakron.edu. Phone: 330-972-2096. Fax: 330-972-5856 (J.Z.).

ORCID

Xiong Gong: 0000-0001-6525-3824

Jie Zheng: 0000-0003-1547-3612

Author Contributions

⊥R.H. and B.R. contributed equally to this work. R.H., B.R., M.Z., H.C., Y.L., B.J., and J.M. carried out the experiments. All authors designed the experiments, interpreted the results, and prepared the manuscript. All authors have given approval to the final version of the manuscript.

Notes

The authors declare no competing financial interest.

ACKNOWLEDGMENTS

This work is financial supported by the NSF (CBET-1510099), Alzheimer Association New Investigator Research Grant (2015-NIRG-341372), and National Natural Science Foundation of China (NSFC-21528601) and partially supported by the NSF (DMR-1607475).

REFERENCES

(1) Bedrood, S.; Li, Y.; Isas, J. M.; Hegde, B. G.; Baxa, U.; Haworth, I. S.; Langen, R. Fibril structure of human islet amyloid polypeptide. *J. Biol. Chem.* **2012**, *287*, 5235−5241.

(2) Cheng, B.; Liu, X.; Gong, H.; Huang, L.; Chen, H.; Zhang, X.; Li, C.; Yang, M.; Ma, B.; Jiao, L.; Zheng, L.; Huang, K. Coffee components inhibit amyloid formation of human islet amyloid polypeptide in vitro: Possible link between coffee consumption and diabetes mellitus. *J. Agric. Food Chem.* **2011**, *59*, 13147−13155.

(3) Lee, C.-C.; Nayak, A.; Sethuraman, A.; Belfort, G.; McRae, G. J. A three-stage kinetic model of amyloid fibrillation. *Biophys. J.* **2007**, *92*, 3448−3458.

(4) Roberts, C. J. Non-native protein aggregation kinetics. *Biotechnol. Bioeng.* **2007**, *98*, 927−938.

(5) Knowles, T. P. J.; Vendruscolo, M.; Dobson, C. M. The amyloid state and its association with protein misfolding diseases. *Nat. Rev. Mol. Cell Biol.* **2014**, *15*, 384−396.

(6) Kayed, R.; Lasagna-Reeves, C. A. Molecular mechanisms of amyloid oligomers toxicity. *J. Alzheimer's Dis.* **2013**, *33*, S67−S78.

(7) Laganowsky, A.; Liu, C.; Sawaya, M. R.; Whitelegge, J. P.; Park, J.; Zhao, M.; Pensalfini, A.; Soriaga, A. B.; Landau, M.; Teng, P. K.; Cascio, D.; Glabe, C.; Eisenberg, D. Atomic view of a toxic amyloid small oligomer. *Science* **2012**, *335*, 1228−1231.

(8) Fändrich, M. Oligomeric intermediates in amyloid formation: Structure determination and mechanisms of toxicity. *J. Mol. Biol.* **2012**, *421*, 427−440.

(9) Levine, H. Thioflavine T interaction with synthetic Alzheimer's disease β-amyloid peptides: Detection of amyloid aggregation in solution. *Protein Sci.* **1993**, *2*, 404−410.

(10) Fink, A. L. Protein aggregation: Folding aggregates, inclusion bodies and amyloid. *Folding Des.* **1998**, *3*, R9−R23.

(11) Chiti, F.; Dobson, C. M. Protein misfolding, functional amyloid, and human disease. *Annu. Rev. Biochem.* **2006**, *75*, 333−366.

(12) Jarrett, J. T.; Berger, E. P.; Lansbury, P. T., Jr. The carboxy terminus of the β amyloid protein is critical for the seeding of amyloid formation: Implications for the pathogenesis of Alzheimer's disease. *Biochemistry* **1993**, *32*, 4693−4697.

(13) Jarrett, J. T.; Lansbury, P. T. Seeding "one-dimensional crystallization" of amyloid: A pathogenic mechanism in Alzheimer's disease and scrapie? *Cell* **1993**, *73*, 1055−1058.

(14) Kayed, R.; Bernhagen, J.; Greenfield, N.; Sweimeh, K.; Brunner, H.; Voelter, W.; Kapurniotu, A. Conformational transitions of islet amyloid polypeptide (IAPP) in amyloid formation in vitro. *J. Mol. Biol.* **1999**, *287*, 781−796.

(15) Come, J. H.; Fraser, P. E.; Lansbury, P. T. A kinetic model for amyloid formation in the prion diseases: Importance of seeding. *Proc. Natl. Acad. Sci. U.S.A.* **1993**, *90*, 5959−5963.

(16) Harper, J. D.; Lansbury, P. T., Jr. Models of amyloid seeding in Alzheimer's disease and scrapie: Mechanistic truths and physiological consequences of the time-dependent solubility of amyloid proteins. *Annu. Rev. Biochem.* **1997**, *66*, 385−407.

(17) Marzaro, M.; Conconi, M. T.; Perin, L.; Giuliani, S.; Gamba, P.; De Coppi, P.; Perrino, G. P.; Parnigotto, P. P.; Nussdorfer, G. G. Autologous satellite cell seeding improves in vivo biocompatibility of homologous muscle acellular matrix implants. *Int. J. Mol. Med.* **2002**, *10*, 177−182.

(18) Luk, K. C.; Kehm, V.; Carroll, J.; Zhang, B.; O'Brien, P.; Trojanowski, J. Q.; Lee, V. M.-Y. Pathological α-synuclein transmission initiates Parkinson-like neurodegeneration in nontransgenic mice. *Science* **2012**, *338*, 949−953.

(19) Luk, K. C.; Kehm, V. M.; Zhang, B.; O'Brien, P.; Trojanowski, J. Q.; Lee, V. M. Y. Intracerebral inoculation of pathological α-synuclein initiates a rapidly progressive neurodegenerative α-synucleinopathy in mice. *J. Exp. Med.* **2012**, *209*, 975−986.

(20) Kane, M. D.; Lipinski, W. J.; Callahan, M. J.; Bian, F.; Durham, R. A.; Schwarz, R. D.; Roher, A. E.; Walker, L. C. Evidence for seeding of β-amyloid by intracerebral infusion of Alzheimer brain extracts in β-amyloid precursor protein-transgenic mice. *J. Neurosci.* **2000**, *20*, 3606−3611.

(21) Holmes, B. B.; Furman, J. L.; Mahan, T. E.; Yamasaki, T. R.; Mirbaha, H.; Eades, W. C.; Belaygorod, L.; Cairns, N. J.; Holtzman, D. M.; Diamond, M. I. Proteopathic tau seeding predicts tauopathy in vivo. *Proc. Natl. Acad. Sci. U.S.A.* **2014**, *111*, E4376−E4385.

(22) Atsmon-Raz, Y.; Miller, Y. Non-Amyloid-β Component of Human α-Synuclein Oligomers Induces Formation of New Aβ Oligomers: Insight into the Mechanisms That Link Parkinson's and Alzheimer's Diseases. *ACS Chem. Neurosci.* **2016**, *7*, 46−55.

(23) Atsmon-Raz, Y.; Miller, Y. Molecular Mechanisms of the Bindings between Non-Amyloid β Component Oligomers and Amylin Oligomers. *J. Phys. Chem. B* **2016**, *120*, 10649−10659.

(24) Baram, M.; Atsmon-Raz, Y.; Ma, B.; Nussinov, R.; Miller, Y. Amylin−Aβ oligomers at atomic resolution using molecular dynamics simulations: A link between type 2 diabetes and Alzheimer's disease. *Phys. Chem. Chem. Phys.* **2016**, *18*, 2330−2338.

(25) Guo, J. L.; Covell, D. J.; Daniels, J. P.; Iba, M.; Stieber, A.; Zhang, B.; Riddle, D. M.; Kwong, L. K.; Xu, Y.; Trojanowski, J. Q. Distinct α-synuclein strains differentially promote tau inclusions in neurons. *Cell* **2013**, *154*, 103−117.

(26) Waxman, E. A.; Giasson, B. I. Induction of intracellular tau aggregation is promoted by α-synuclein seeds and provides novel insights into the hyperphosphorylation of tau. *J. Neurosci.* **2011**, *31*, 7604−7618.

(27) Charles, V.; Mezey, E.; Reddy, P. H.; Dehejia, A.; Young, T. A.; Polymeropoulos, M. H.; Brownstein, M. J.; Tagle, D. A. α-Synuclein immunoreactivity of huntingtin polyglutamine aggregates in striatum and cortex of Huntington's disease patients and transgenic mouse models. *Neurosci. Lett.* **2000**, *289*, 29−32.

(28) Andreetto, E.; Yan, L.-M.; Tatarek-Nossol, M.; Velkova, A.; Frank, R.; Kapurniotu, A. Identification of hot regions of the Aβ−IAPP interaction interface as high-affinity binding sites in both cross- and self-association. *Angew. Chem., Int. Ed.* **2010**, *49*, 3081−3085.

DOI: 10.1021/acsomega.6b00559
ACS Omega 2017, 2, 784−792

(29) Yan, L.-M.; Velkova, A.; Tatarek-Nossol, M.; Andreetto, E.; Kapurniotu, A. IAPP mimic blocks Aβ cytotoxic self-assembly: Cross-suppression of amyloid toxicity of Aβ and IAPP suggests a molecular link between Alzheimer's disease and type II diabetes. *Angew. Chem., Int. Ed.* **2007**, *46*, 1246−1252.
(30) Mandal, P. K.; Pettegrew, J. W.; Masliah, E.; Hamilton, R. L.; Mandal, R. Interaction between Aβ peptide and α synuclein: Molecular mechanisms in overlapping pathology of Alzheimer's and Parkinson's in dementia with Lewy body disease. *Neurochem. Res.* **2006**, *31*, 1153−1162.
(31) Giasson, B. I.; Forman, M. S.; Higuchi, M.; Golbe, L. I.; Graves, C. L.; Kotzbauer, P. T.; Trojanowski, J. Q.; Lee, V. M.-Y. Initiation and synergistic fibrillization of tau and α-synuclein. *Science* **2003**, *300*, 636−640.
(32) Vagelatos, N. T.; Eslick, G. D. Type 2 diabetes as a risk factor for Alzheimer's disease: The confounders, interactions, and neuropathology associated with this relationship. *Epidemiol. Rev.* **2013**, *35*, 152−160.
(33) Morales, R.; Moreno-Gonzalez, I.; Soto, C. Cross-seeding of misfolded proteins: Implications for etiology and pathogenesis of protein misfolding diseases. *PLoS Pathog.* **2013**, *9*, No. e1003537.
(34) Morales, R.; Estrada, L. D.; Diaz-Espinoza, R.; Morales-Scheihing, D.; Jara, M. C.; Castilla, J.; Soto, C. Molecular cross talk between misfolded proteins in animal models of Alzheimer's and prion diseases. *J. Neurosci.* **2010**, *30*, 4528−4535.
(35) O'Nuallain, B.; Williams, A. D.; Westermark, P.; Wetzel, R. Seeding specificity in amyloid growth induced by heterologous fibrils. *J. Biol. Chem.* **2004**, *279*, 17490−17499.
(36) Du, J.; Cho, P. Y.; Yang, D. T.; Murphy, R. M. Identification of beta-amyloid-binding sites on transthyretin. *Protein Eng., Des. Sel.* **2012**, *25*, 337−345.
(37) Ribeiro, C. A.; Oliveira, S. M.; Guido, L. F.; Magalhães, A.; Valencia, G.; Arsequell, G.; Saraiva, M. J.; Cardoso, I. Transthyretin Stabilization by Iododiflunisal Promotes Amyloid-β Peptide Clearance, Decreases its Deposition, and Ameliorates Cognitive Deficits in an Alzheimer's Disease Mouse Model. *J. Alzheimers Dis.* **2014**, *39*, 357−370.
(38) Cao, P.; Abedini, A.; Raleigh, D. P. Aggregation of islet amyloid polypeptide: From physical chemistry to cell biology. *Curr. Opin. Struct. Biol.* **2013**, *23*, 82−89.
(39) Zhang, M.; Hu, R.; Chen, H.; Chang, Y.; Gong, X.; Liu, F.; Zheng, J. Interfacial interaction and lateral association of cross-seeding assemblies between hIAPP and rIAPP oligomers. *Phys. Chem. Chem. Phys.* **2015**, *17*, 10373−10382.
(40) Zhang, M.; Hu, R.; Liang, G.; Chang, Y.; Sun, Y.; Peng, Z.; Zheng, J. Structural and energetic insight into the cross-seeding amyloid assemblies of human IAPP and rat IAPP. *J. Phys. Chem. B* **2014**, *118*, 7026−7036.
(41) Hu, R.; Zhang, M.; Patel, K.; Wang, Q.; Chang, Y.; Gong, X.; Zhang, G.; Zheng, J. Cross-sequence interactions between human and rat islet amyloid polypeptides. *Langmuir* **2014**, *30*, 5193−5201.
(42) Profit, A. A.; Felsen, V.; Chinwong, J.; Mojica, E.-R. E.; Desamero, R. Z. B. Evidence of π-stacking interactions in the self-assembly of hIAPP22-29. *Proteins: Struct., Funct., Bioinf.* **2013**, *81*, 690−703.
(43) Tenidis, K.; Waldner, M.; Bernhagen, J.; Fischle, W.; Bergmann, M.; Weber, M.; Merkle, M.-L.; Voelter, W.; Brunner, H.; Kapurniotu, A. Identification of a penta- and hexapeptide of islet amyloid polypeptide (IAPP) with amyloidogenic and cytotoxic properties. *J. Mol. Biol.* **2000**, *295*, 1055−1071.
(44) Nilsson, M. R.; Raleigh, D. P. Analysis of amylin cleavage products provides new insights into the amyloidogenic region of human amylin. *J. Mol. Biol.* **1999**, *294*, 1375−1385.
(45) Green, J.; Goldsbury, C.; Mini, T.; Sunderji, S.; Frey, P.; Kistler, J.; Cooper, G.; Aebi, U. Full-length rat amylin forms fibrils following substitution of single residues from human amylin. *J. Mol. Biol.* **2003**, *326*, 1147−1156.
(46) Hoffmann, K. Q.; McGovern, M.; Chiu, C.-c.; de Pablo, J. J. Secondary structure of rat and human amylin across force fields. *PLoS One* **2015**, *10*, No. e0134091.
(47) Dahlgren, K. N.; Manelli, A. M.; Stine, W. B., Jr.; Baker, L. K.; Krafft, G. A.; LaDu, M. J. Oligomeric and fibrillar species of amyloid-β peptides differentially affect neuronal viability. *J. Biol. Chem.* **2002**, *277*, 32046−32053.

DOI: 10.1021/acsomega.6b00559
ACS Omega 2017, 2, 784−792